# Water Surface is Acidic

**Victoria Buch,[1] Anne Milet,[2] Robert Vácha,[3] Pavel Jungwirth,[3*] and J. Paul Devlin[4]**

*[1]Fritz Haber Institute for Molecular Dynamics, Hebrew University, Jerusalem, Israel 91904, [2]LEDSS, Université Joseph Fourier, BP53, 38041 Grenoble , France, [3]Institute of Organic Chemistry and Biochemistry, Academy of Sciences Sciences of the Czech Republic and Center for Biomolecules and Complex Molecular Systems, 16610 Prague 6, Czech Republic, [4]Department of Chemistry, Oklahoma State University, Stillwater, Oklahoma 74078, USA*

**Classification:** Physical Sciences - Chemistry

**Manuscript Information:** 21 (double spaced) pages, 4 figures, and 0 tables. Number of words in the abstract: 150. Total number of characters in the paper (including spaces): 36184.

**Keywords:** water surface, autoionization, surface pH, molecular dynamics, density functional theory, IR spectroscopy.

*[*]To whom correspondence should be addressed: Pavel.Jungwirth@uochb.cas.cz*

**Abstract**

Water autoionization reaction $2H_2O \rightarrow H_3O^+ + OH^-$ is a textbook process of basic importance, resulting in pH = 7 for pure water. However, pH of pure water *surface* is shown to be significantly lower, the reduction being due to proton stabilization at the surface. The evidence presented here includes *ab initio* and classical molecular dynamics simulations of water slabs with solvated $H_3O^+$ and $OH^-$ ions, density functional studies of $(H_2O)_{48}H^+$ clusters, and spectroscopic isotopic-exchange data for $D_2O$ substitutional impurities at the surface and in the interior of ice nanocrystals. Since $H_3O^+$ does but $OH^-$ does not display preference for surface sites, the $H_2O$ surface is predicted to be acidic with pH lower than 4.8. For similar reasons, the strength of some weak acids such as carbonic acid is expected to increase at the surface. Enhanced surface acidity can have a significant impact on aqueous surface chemistry, e.g., in the atmosphere.

## Introduction

In room temperature liquid, one in $6 \cdot 10^8$ water molecules is autoionized, yielding the standard value of pH = 7. Autoionization in crystal ice should be less favourable, since, in contrast to water, ice is a very poor solvent of ionic and polar substances *(1)*. As recently realized *(2-5)*, chemistry and composition of aqueous surfaces is quite distinct from that of the bulk, therefore, autoionization behaviour should be re-examined at the *surface*.

A number of recent computations *(6-8)* indicated preference of hydronium cations for surface positions. Surface propensity of $H_3O^+$ was also deduced from vibrational spectroscopy of large protonated water clusters *(6),* as well as vibrational sum frequency generation (VSFG) *(8,9)* and second harmonic generation (SHG) *(10)* spectroscopic experiments probing extended aqueous interfaces. Interestingly, zeta potential measurements and titration experiments on oil droplets dispersed in water indicated the presence of negative charges at the interface, interpreted as adsorbed $OH^-$ ions *(11)*. Similar conclusions have also been drawn from zeta potentials of air bubbles in water *(12)*. More work is clearly needed to reconcile this apparent discord between predictions of surface selective spectroscopies and molecular simulations on one side and electrochemical measurements on the other side.

$H_3O^+$ forms three strong proton-donor bonds to $H_2O$, but acts as a poor proton acceptor. A surface position with only H-atoms hydrogen bonded is preferred to interior positions, because the latter are associated with disruption of the approximately tetrahedral hydrogen bond network in water *(10)*. The present work focuses on the effect of surface stabilization of hydronium on water autoionization and on surface pH.

## Calculations

*Overview:* Modeling of proton-tranfer systems is a non-trivial problem, since standard (empirical) potential energy surfaces do not include a possibility of proton hopping between different water molecules, or transitions between the two limiting protonated water forms (the hydronium $H_3O^+$ and the Zundel ion $H_2O..H^+..OH_2$). In the present study, three complementary computational approaches were employed. First, NVT *ab initio* molecular dynamics simulations were carried out for liquid water with a pair of $H_3O^+$ and $OH^-$ ions. To assess surface effects, the simulation was carried out both for a box with three-dimensional periodic boundaries, and for a slab with two open surfaces and two-dimensional periodic boundaries. This "on-the-fly" technique enables first-principle modeling of proton transfer systems at finite temperatures; proton transfer and transitions between the different protonated-water forms are automatically included in the computational scheme. However the high computational cost limits the dimensionality of the model system, the duration of the trajectories, and the accuracy of the electronic structure method used to evaluate the forces and the energies.

Direct simulation of autoionization is not easily feasible due to the activation barrier (see, however, a pioneering study of bulk autoionization in Ref. 13). On the other hand, recombination between $H_3O^+$ and $OH^-$can be readily observed in on-the-fly simulations, on a feasible time scale, enabling qualitative assessment of the autoionization energetics. On-the-fly results suggest a significant lowering of the endothermicity of the autoiozation reaction at the surface, with respect to the bulk, due to the stabilization of the protonated water at the interface.

To assess more quantitatively the extent of this stabilization, *ab initio* techniques were applied to calculate the energy of a protonated water cluster $(H_2O)_{48}H^+$ with the proton either at the surface or in the interior. At this size, fairly accurate electronic

structure calculations can be made for the system energetics. The calculations indicated substantial energy lowering upon proton transfer from the interior to the surface of the cluster. However, behavior of an aqueous solution is ultimately determined by the free energy (rather than the energy) difference between the interior and the surface ion states. Calculations of the free energy differences ( $\Delta G_{sb}$ ) between these states are feasible only with empirical potentials. Such calculations were performed in the third part of the study, for aqueous solutions in slab geometry of protonated-water ions in the two limiting forms (hydronium and Zundel), and of the hydroxide ion. Polarizable potentials were employed, which were calibrated against cluster *ab initio* data. In this part, the use of potential models which do not include proton tranfer is reasonable since a thermodynamic rather than a dynamic quality is calculated. The resulting $\Delta G_{sb}$ values were consistent with enhanced acidity of the neat water surface, due to proton preference for the surface, and lack thereof for the hydroxide. The different computations are described in more detail below.

*On-the-fly dynamics:* NVT classical trajectories were evaluated at 270 K. The nuclei moved on the Born-Oppenheimer potential energy surface, which was calculated at each time step at the BLYP/DZVP level of the density functional theory (DFT). CP2K/QUICKSTEP package was employed *(14);* see caption of Fig. 1 and "Computational methods" for further technical details. First, a single ion ($H_3O^+$ or $OH^-$ ) was simulated in an 11 Å thick water slab containing 71 water molecules. Throughout a 2.5 picosecond simulation, the cation remained at the surface. In a similar simulation, the anion underwent initially several quick proton transfer cycles between the surface and the interior, but after 0.3 ps settled in the interior of the slab for the remainder of the simulation. The latter result is consistent with recent SFG data and simulations employing an empirical potential, which indicated lack of surface preference for hydroxide *(8, 9)*.

Simulation of a slab including both of the ions ($H_3O^+$ and $OH^-$ ) required some effort, since, due to the limited dimensionality of the model, the ions tended to recombine before relaxing. Different initial locations were tried for the two ions. Finally, a trajectory was generated in which the two ions acquired favorable solvation shells prior to recombining and thus survived for the duration of 5.4 ps. During the first picosecond of this trajectory, the two ions formed an interesting solvent-separated ion-pair, with the central water molecule acting as proton acceptor with respect to both ions. (In this configuration, recombination is blocked by the central water molecule; such configurations may in fact serve as intermediates in the autoionization process in water.) During this part of the trajectory, the ion pair resided in the slab interior; however the proton underwent numerous back-and-fort transitions between the ion-pair configuration and the surface. At t ~ 1 ps, the two ions separated; the proton moved to the surface, while the hydroxide adopted an interior position. The ions remained so until just before recombination (t ~ 5.3 ps), at which time the anion emerged at the surface.

Figure 1 (A) shows the energy of the system along the trajectory, together with energy for a trajectory of a neutral water slab without the ions. The two energies are the same within the accuracy of the calculation. The energy difference between the autoionized and neutral system cannot be assessed quantitatively from this calculation, because of the large potential energy fluctuations of the finite dimensionality systems, and also due to the limited accuracy of the DFT/BLYP method. However one may note the qualitative difference with respect to a bulk on-the-fly simulation, employing cubic three-dimensional periodic boundaries, for which the energy of the autoionized system clearly exceeded the energy of the neutral one (Fig. 1(B)). Note in Fig. 1(B) that the drop in potential energy is delayed by 1 ps with respect to recombination, marked by the arrow, since the surrounding water molecules need some time to relax to the new environment of the recombined ion pair. The above on-the-fly results are consistent with

preference of protonated water for surface sites, and suggest reduced endothermicity of autionization at the liquid surface due to surface stabilization of the cation.

*Search for low energy structures of the $(H_2O)_{48}H^+$ cluster:* Since $OH^-$ does not display surface preference, the crucial quantity for the present argument is the free energy lowering as the proton is moved from the $H_2O$ bulk to the surface. The main contribution is expected to originate from the energy change due to surface stabilization of the proton. To estimate the energy change, a search was made for low energy structures of a protonated water cluster $(H_2O)_{48}H^+$, with the proton either on the surface or in the interior. At this size, B3LYP calculations can be made of the system energetics. B3LYP method is expected to yield much more accurate energy values than BLYP used in the slab and bulk calculations; as a matter of fact, this method benchmarked very well against more accurate *ab initio* calculations for autoionization in the water octamer *(15)*.

The initial search for low energy cluster structures employed a molecular dynamics-based method described in Ref. 16. NVE trajectories lasting several nanoseconds were run for the cluster at a mean temperature of ~200 K. At this stage, the calculation employed a non-polarizable empirical potential for the hydronium-water system (8). Trajectory structures were minimized every 5 ps. A bank of ~1200 perspective minima was thus obtained, with the hydronium either at the cluster surface, or in the interior. The energies of the minima were then recalculated at the BLYP/DZVP level, following a single minimization step. Ten thus-obtained lowest energy structures of each kind (i.e., with the proton at the surface or in the bulk) were subjected to full minimization at the BLYP/DZVP level. The final energies were then recalculated at the B3LYP level. The average energy difference between the 10 lowest energy minima with the proton in the interior and the 10 lowest energy minima with the proton at the surface was 8.7 kcal/mol and 10.5 kcal/mol, for B3LYP and BLYP, respectively. Three of the lowest energy minima of each kind were furthermore fully reoptimized at the B3LYP

level; resulting in 8.8 kcal/mol energy difference between a pair of lowest energy minima of each kind. This energy preference for surface structures is consistent with the values obtained by other authors for smaller $(H2O)_{n=20,21}H^+$ clusters *(6,7)* which, however, acquire a rather special cage-like geometry.

*Calculations of $\Delta G_{sb}$:* Finally, to assess the surface preferences of protonated and deprotonated water, *free*-energy differences $\Delta G_{sb}$ between the bulk and the surface, for the respective ions, are needed. For that purpose, simulations employing thermodynamic integration were carried out for each ion dissolved in a slab of liquid water. The scope of these simulations necessitated the use of computationally efficient empirical potentials, which were calibrated against ab initio MP2/aug-cc-pvdz geometries and energies of small water clusters with $H_3O^+$ or $OH^-$. For further computational details, see caption to Fig. 2 and "Computational methods". For $H_3O^+$, the calculation predicted a free-energy preference for the surface of ~3 kcal/mol. This value is likely a lower bound, since the empirical potential underestimates, with respect to B3LYP, the average energy difference between "in" and "out" structures of $(H_2O)_{48}H^+$ clusters, yielding an average energy difference of ~4 kcal/mol. Thus, $\Delta G_{sb}$ of the proton deduced from the empirical potential could be too small by up to 4 kcal/mol, due to the underestimation of this energy difference. Additional $\Delta G_{sb}$ calculations employing an empirical potential were carried out for the proton-sharing Zundel form of protonated water $H_2O..H^+..OH_2$; the $\Delta G_{sb}$ value obtained in the simulation was similar to that of the $H_3O^+$ ion. (Zundel ions were examined, since according to our on-the-fly calculations, about 30% of protonated water configurations resemble the Zundel rather than the $H_3O^+$ ion). In contrast to hydrated proton, no surface preference was found for $OH^-$, which weakly prefers the bulk with $\Delta G_{sb}$ of -1 to -2 kcal/mol. A typical snapshot depicting a surface bound $H_3O^+$ and bulk $OH^-$ is shown in Fig. 2.

Using the above lower bound of the proton surface stability $\Delta G_{sb}$ = 3 kcal/mol, one obtains at 300K a ~150-fold increase in surface concentration of $H_3O^+$ compared to the bulk. (This is a larger surface enhancement then observed in our previous MD simulations *(8)*, which is mainly due to a refined potential and lower $H_3O^+$ concentration in this study.) This translates to pH ~4.8 of the top-most layer of neat water (as usual, we define pH as the negative logarithm of proton concentration rather than of its activity, which is justified at these low ion concentrations). Assuming the above upper bound $\Delta G_{sb}$ value for $H_3O^+$ suggests surface pH possibly as low as 1.9. At the same time, the surface pOH is estimated as 7.7 - 8.4. We thus conclude that the surface of pure water is acidic.

**Experiment**

Additionally, we present experimental evidence that ice nanocrystal surfaces are slightly acidic, similarly to liquid $H_2O$ surfaces. Proton activity in ice can be monitored by observation of isotopic exchange *(17-20)*, since the only known mechanism of the reaction $D_2O + H_2O \rightarrow 2HDO$ at experimental temperatures is via proton transfer *(1)*. In the absence of acidic impurities, the protons are provided by $H_2O$ autoionization. ($OH^-$ contribution to the exchange is much less than that of the proton, due to a significantly lower mobility *(21)*, i.e., no isotopic exchange is observed in thick ice films grown from the vapour of very dilute ammonia-water solutions on a time scale of days at 155 K.) In the interpretation of the experimental data, advantage is taken of some of the computational results presented above. To justify that, we note that ice nanocrystals were shown to include a ~5 angstrom thick disordered surface layer, and a partially disordered subsurface layer (22). Thus it is reasonable to surmise that surface and subsurface states of the proton at the disordered nanoparticle surface are similar to those of the amorphous

$(H_2O)_{48}H^+$ cluster, and of a cold liquid. On the other hand, *interior* proton states are expected to be more unfavorable inside the nanocrystal than inside $(H_2O)_{48}H^+$ or the liquid. This is since in contrast to the liquid, crystal ice is a very poor solvent *(1)*.

*Experimental technique:* Infrared spectroscopic observation of isotopic exchange in/on ice nanoparticles in the 110-150 K temperature range was carried out much as described in Ref. 18. Aerosols of $H_2O$ particles, with an average diameter in the 12 - 40 nm range, were prepared containing small percentages of intact $D_2O$. Gas pulses from two separate one-liter He(g) reservoirs with the same total gas pressure, one containing 1.0 % of $H_2O$ and the other ~0.1 % of $D_2O$, were transmitted via co-axial tubing to the inside of a double-walled cold-condensation cell. Simultaneous release and thorough overlap of the gas pulses allowed ice nanocrystals to form with nearly uniform distribution of $D_2O$ between and within the particles. Significant H-D exchange occurred during gas handling and within the cold-droplet phase of the nanocrystal formation process, but typically every second or third deuterium appeared as intact isolated $D_2O$ (as exemplified by the solid-line spectrum in the right panel of Fig 3).

Ultimately, the ability to monitor the exchange rates is based on distinct spectroscopic signatures of isotopically isolated $D_2O$ and HDO (Fig. 3). Upon passage of a mobile proton defect, an isolated $D_2O$ is converted to an HDO neighbour pair, and subsequently, through successive molecular-turn and proton-hop steps, to isolated HDO *(1, 17)*). Fig. 3 displays typical spectroscopic results for exchange rates at the ice nanocrystal surfaces, and in their interiors. Note that we rely on opportune presence of distinct and well-spaced spectroscopic features for the two environments. The assignment of the three distinct interior bands near 2400 $cm^{-1}$ (right panel, Fig. 3) to isolated $D_2O$ (symmetric stretch - 2370 $cm^{-1}$; asymmetric stretch - 2447 $cm^{-1}$) and isolated HDO (2420 $cm^{-1}$) within ice has been thoroughly documented *(1,17)*.

Similarly, surface free-OH and free-OD stretch bands have been studied in detail *(22)* and used by us and others in numerous investigations of ice surface adsorbates. In particular, the two free-OD surface bands (left panel, Fig. 3), one of $D_2O$ (2725 $cm^{-1}$) and the other of HDO (2712 $cm^{-1}$), have been used to demonstrate the preference for D-bonding over H-bonding of the single-donor surface HDO molecules *(23)*. Identification of the HDO surface spectrum in the absence of $D_2O$ was made using nanocrystals prepared from premixed $H_2O$ with <5% $D_2O$. The temperature-dependent preference of single-donor HDO to D-bond at temperatures used in this study limits the value of the 2712 $cm^{-1}$ band as a measure of isotopic exchange (23). Therefore, quantitative rates for the surface exchange have been deduced from the decrease in the 2725 $cm^{-1}$ $D_2O$ band (see Fig. 4).

*Results:* Isotopic exchange in the ice nanocrystal interior occurs on the time scale of minutes to hours in the 150 - 130 K range, much as observed for thick ice films *(17, 18). On the surface, the relative initial rate is ~20 times faster*, as deduced from data such as in Fig. 3 and 4. In the example of Fig. 3 for temperatures near 140 K, the surface exchange is nearly complete in 90 s during which time period the interior exchange is <10%. Figure 4 shows graphically the percent loss with time of the interior $D_2O$ asymmetric- stretch band intensity and the diminution of the normalized peak intensity of the free-O-D surface band of $D_2O$ for a sample held at 128K for 18 minutes. The latter decrease indicates a half-life of ~7 minutes, while the decrease of the interior $D_2O$ band by 7.8% over 18 minutes extrapolates to a half-life of 154 minutes (assuming a first order exchange process). This result, typical of kinetic runs for numerous aerosols of "pure" ice nanocrystals, suggests a ratio of 22 for the respective rates. However, initial results, for the temperature dependence of the surface exchange rates, point to an activation energy of 5 kcal/mol which can be contrasted with a value of ~9 kcal/mol reported for H-D

exchange within micron-thick ice films *(1, 17).* Thus the ratio of rates, surface-to-interior, are expected to decrease with increasing temperature.

The ~20 ratio of surface-to-interior exchange rates indicates enhanced proton concentration at the surface and/or enhanced mobility at the surface. We shall argue here in favour of the first possibility. As noted above, ice nanocrystals were shown in the past to have disordered surfaces *(22)*, and one expects lower mobility in the disordered medium (surface) than in the crystal one (interior). For example, it has been established that no proton transfer occurs in *pure* compacted amorphous ice below 140K, and that, relative to crystalline ice, a greater abundance of injected protons is required to induce H-D exchange at ~120K *(24)*. Because of the surface and subsurface disorder, protonated $H_2O$ configurations there should be similar to those in amorphous ice, liquid water, and the amorphous $(H_2O)_{48}H^+$ cluster. On the other hand, proton transfer from the surface to the crystalline bulk is expected to be more endothermic than for the liquid, since, in contrast to water, crystal ice is a very poor solvent *(1,25)*. Further, one may note past computational results favoring a greater surface than bulk proton concentration, which showed that the O..H interaction between hydronium embedded in ice, and the proton-donating neighbor water molecule is repulsive *(26)*.

The effect of surface impurities on the relative isotopic exchange rates is revealing. 20% of a surface monolayer (ML) of $H_2S$ enhances both the surface and interior exchange rate by only a factor ~2.5. Thus at the surface the autoionization constant of water is of the same order of magnitude as $K_a$ of $H_2S$, which is a weak acid. On the other hand, paralleling reports for thick ice films *(21)*, a small amount of $NH_3$ adsorbate (< 1% of an ML) stops the isotopic exchange altogether on the time scale of the experiment (~1/2 hour), evidently due to proton trapping by the base. The exchange in the interior resumes when the ammonia coverage is increased to beyond 10% of an ML and, with coverage >50% of an ML, the rate exceeds that of pure ice. *However, now the*

*surface exchange rate is no longer enhanced with respect to the interior.* The larger amounts of ammonia generate sufficient $OH^-$ so that isotopic exchange takes place despite its reduced mobility with respect to the proton *(21)*.

Due to the poor solvation properties of crystal ice, one still expects $OH^-$ to spend most of the time in non-crystalline portions of the particle. In characterization of the structures of ice nanoparticles, it has been noted that there exists a significantly distorted surface and subsurface region with a thickness of ~1 nm (see, for example, pages 400 - 403 of ref 22). The computational results suggest that $OH^-$ favours the subsurface region rather than surface sites. Accordingly, the exchange induced by a large amount of $NH_3$ does not display any isotopic exchange enhancement of the surface, with respect to the bulk, in contrast to the pure $H_2O$ nanoparticles. Acidity of the nanocrystal surface is a combined outcome of surface sites for the protons and subsurface sites for $OH^-$.

Considering that the subsurface region differs from both the surface and the interior of the nanocrystals, it is likely that the exchange rates of that region are also unique. Kang et al have reported reactive-ion-scattering data that are consistent with a greater exchange rate in the subsurface of *amorphous* ice films than for the bulk *(19)*. Since the nanocrystal subsurface has a distinct infrared spectrum *(22)*, the possibility exists for extension of our methods to determination of the exchange rates for this third component of the nanocrystals. However, with the present study based on relatively large nanocrystals, the subsurface $D_2O$/HDO bands are present as small broad components directly underlying the interior ice spectra. Studies with still smaller particles for which the subsurface bands rival the interior-ice band intensities (as for 4 nm diameter crystals as displayed in Figs. 2 and 4 of ref. 22) may permit identification of the exchange rates within the subsurface.

## Conclusions

Based on molecular computational and experimental evidence we have shown that the surface of neat water is acidic with pH lower than 4.8 due to a significant surface propensity of hydronium (but not hydroxide) ions. By argument analogous to our results for neat water, weak acid solutions can display enhanced surface acidity, i.e., surface pH reduction by at least 2.2 units, corresponding to $\Delta G_{sb} \geq 3$ kcal/mol of hydrated protons. (Note that pKa of the acid is not necessarily reduced by the same extent, being affected additionally by $\Delta G_{sb}$ values of the neutral acid, and of the negative ion *(27-29)*.) The case of carbonic acid is of particular interest. Under normal atmospheric conditions, bulk water exposed to the air acquires pH of 5.7 since some of the dissolved $CO_2$ gas undergoes a reaction $CO_2 + 2\ H_2O \rightarrow H_3O^+ + HCO_3^-$. At the surface, pH will be reduced more significantly than in the bulk, due to surface propensity of hydronium ions. Enhanced acidity of water surface can have a significant impact on aqueous surface chemistry in natural atmospheric environments, cloud nucleation, thundercloud electrification, and electrochemistry (e.g., corrosion processes).

As noted in the Introduction, the present results are in contradiction with the microscopic interpretation proposed for macroscopic titration experiments and zeta potential measurements on oil emulsions and gas bubbles in water *(11,12)*. These experiments indicated negatively charged surfaces. It was proposed that this effect is due to a substantial surface propensity of $OH^-$ and lack thereof for $H_3O^+$. The existing controversy between molecular simulations and spectroscopic experiments on one side and macroscopic measurements on the other side, which probably cannot be fully resolved at the moment, will be discussed in detail in our forthcoming review publication *(30)*.

**Computational details**

The *ab initio* molecular dynamics simulations employed an on-the-fly NVT code as implemented in the CP2K/QUICKSTEP package *(14*). The scheme combines a Gaussian basis for the wave functions with an auxiliary plane wave basis set for the density. The DFT/BLYP functional was used in conjunction with the DZVP basis, and pseudopotentials of the Goedecker-Teter-Hutter type *(31).* The time step was 0.5 femtosecond. The first simulation pertained to a slab of 72 water molecules in a 13.47 × 15.56 Å two-dimensional periodic box; the thickness of the slab was ~11 Å. A Martyna-Tuckerman Poisson solver was used in the calculation with 2D periodic boundaries (32). In the simulations with a single ion, one of the surface water molecules was converted initially to either $H_3O^+$ or $OH^-$ by addition or subtraction of an H atom. Additional simulations were carried out for a zwitterionic system, after converting two water molecules to $H_3O^+$ and $OH^-$. The second set of simulations pertained to 64 water molecules in a cubic box of dimension 12.41 Å, with 3D periodic boundaries. For both 3D and 2D periodic boundary conditions long range electrostatic interactions were accounted for via an Ewald summation. For the above computational parameters, the water self-diffusion constant in a 3D box is 2.50 and 0.52 $10^{-5}$ $cm^2s^{-1}$ at 300 and 270 K, respectively, as compared to the experimental values of 2.57 and 1.13 $10^{-5}$ $cm^2s^{-1}$ at 298 and 273 K, respectively *(33,34)*. The simulations were carried out finally at 270 K, since at this temperature it was easier to stabilize the hydronium-hydroxide ion pair within the finite size box.

For the free energy calculations we employed the thermodynamic integration method as implemented in a classical molecular dynamics package Gromacs 3.3.1 *(35)* with a control routine *(36)* ensuring statistical error below a given threshold (~1 kcal/mol). This required nanosecond timescale runs, which were performed in the NVT

(300 K) ensemble using a 1 fs timestep. The slab was formed by placing 432 POL3 *(37)* water molecules, $H_3O^+$ (Eigen) or $H_5O_2^+$ (Zundel) and $OH^-$ into a 3D periodic unit cell of 18.7 × 18.7 × 237 Å. A 9 Å interaction cut off with a particle mesh Ewald sum *(38)* for long range electrostatic interactions was employed. We tested a set of potential parameters for these ions, which we either took from literature *(8)*, or we fitted the van der Waals radius of the oxygen of the ion against ab initio MP2/aug-cc-pvdz geometries and energies of clusters containing $H_3O^+$ or $OH^-$ with three strongly bound water molecules. Alternatively, we aimed to match the energy difference between the surface and bulk located hydronium, as obtained in the above DFT calculations for the $(H_2O)_{48}H^+$ clusters. In either case, we did not allow the ion oxygen radius $H_3O^+$ to deviate more than 10 % from those of the previously employed models *(8)* in order to remain within physically reasonable potential parameters.

---

**Acknowledgement**

Support from the Czech Ministry of Education (grants LC512 and ME644), the Granting Agency of the Czech Republic (grant 202/06/0286), and the US-NSF (grants CHE 0431312 and 0209719) is gratefully acknowledged by PJ. VB and JPD acknowledge the funding of the Israel-US Binational Science Foundation. RV thanks the Granting Agency of the Czech Republic for support via a grant 203/05/H001.

**References**


1. Petrenko, V. F., Whitworth, R. W. *Physics of Ice* (Oxford Univ. Press: Oxford, 1999).

2. Richmond, G. L. (2001) *Ann. Rev. Phys. Chem*. **52**, 357-389.

3. Shultz, M. J., Badelli, S.,Schnitzer, C., Simonelli, D. (2002), *J. Phys. Chem. B* **106**, 5313-5324.

4. Peterson, P. B., Saykally, R. J. (2006) *Ann. Rev. Phys. Chem*. **57**, 333-364.

5. Jungwirth, P., Tobias, D. (2006) *Chem. Rev*. **106**, 1259-1281.

6. Shin, J.W., Hammer, N.I., Diken, E.G., Johnson, M.A., Walters, R.S., Jaeger, T.D., Duncan, M.A., Christie, R.A., Jordan, K.D. (2004) *Science* **304**, 1137-1140.

7. Peterson, M. K., Iyengar, S. S., Day, T. J. F., Voth, G. A. (2004) *J. Phys. Chem B* **108**, 14804-14806.

8. Mucha, M., Frigato, T., Levering, L. M., Allen, H. C., Tobias, D. J., Dang, L. X., Jungwirth, P. (2005) *J. Phys. Chem B* **109**, 7617-7623.

9. Tarbuck, T. L., Ota, S. T.; Richmond, G. L. (2006) *J. Am. Chem. Soc.* **128**,14519-14527.

10. Petersen, P.B., Saykally, R.J. (2005) *J. Phys. Chem. B* **109**, 7976-7980.

11. Beattie, J. K., Djerdjev, A. M. (2004) *Angew. Chem. Int. Ed.* **43,** 3568-3571.

12. Beattie, J. K. (2006) *Lab Chip* **6,** 1409-1411.


.

13. Geissler, P. L., Dellago, C., Chandler, D., Hutter, J., Parrinello, M. (2001) Science 292, 2121-2124.

14. . VandeVondele, J., Krack, M., Mohamed, F., Parrinello, M., Chassaing, T., Hutter, J. (2005) *Computer. Phys. Comm.* **167**, 103-128

15. Svozil, D., Jungwirth, P. (2006) *J. Phys. Chem. A* **2006**, 9194-9199.

16. Buch, V., Martonak, R., Parrinello, M. (2006) *J. Chem. Phys*. **124**, 204705.

17. Devlin, J. P. (1990) *Int. Rev. Phys. Chem.* 9, 29-65.

18. Uras-Aytemiz, N., Joyce, C., Devlin, J. P. (2001) *J. Chem. Phys.* **115**, 9835-9842.

19. Park, S-C.; Jung, K-H.; Kang, H. (2004) *J. Chem. Phys.* **121**, 2765-2774

20. Kang, H. (2005) *Acc. Chem. Res.* **38**, 893-900.

21. Devlin, J. P. in "*Proton Transfer in Hydrogen-Bonded Systems*" NATO ASI Series-Vol. 291, pp 249 - 260, ed. T. Bountis (Plenum Press, New York, 1992).

22. Buch, V., Bauerecker, S., Devlin, J.P., Buck, U., Kazimirski, J.K. (2004) *Int. Rev. Phys. Chem*. **23**, 375-433.

23. Devlin, J. P. (2000) *J. Chem. Phys.* **112**, 5527-5529.

24. Fisher, M., Devlin, J. P. (1995*) J. Phys. Chem***. 99**, 11584 - 11590.

25. Hernandez, J.; Uras, N.; Devlin, J. P. (1998) *J. Phys. Chem. B* **102**, 4526-3535.

26. Kobayashi, C., Saito, S., Ohmine, I. (2000) *J. Chem. Phys.* **113**, 9090-9100.

*27.* Bhattacharyya, K., Sitzmann, E. V., Eisenthal, K. B. (1987) *J. Chem. Phys.* **87**, 1442-1443.

28. Castro, A, Bhattacharyya, K., Eisenthal, K. B. (1991) *J. Chem. Phys.* **95**, 1310-1315.

29. Gopalakrishnan, S., Liu D., F., Allen H. C., Kuo M., Shultz M. J. (2006) *Chem. Rev.* **106**, 1155-1175.

30. Vacha, R., Buch, V., Milet, A., Devlin, J. P., Jungwirth, P. *Phys. Chem. Chem. Phys., to be submitted.*

31. Goedecker, S.; Teter, M.; Hutter, (1996) J. *Phys. Rev. B*, **54,** 1703-1710.

32. Martyna, g. J., Tuckerman, M. E., J. Chem. Phys.(1999) ***110***, 2810-2821.

33. Easteal, A. J.,Price, W. E. and Woolf, L. A., *J. Chem. Soc., Faraday Trans. 1*, (1989), **85**, 1091-1097.

34. Holz, M., Heil, S. R., Sacco, A., *Phys. Chem. Chem. Phys.* (2000), **2,** 4740-4742.

35. Lindahl, E., Hess, B., van der Spoel, D. (2000) *J. Mol. Model.* **7**, 306-317.

36. Kubar, T., Hanus, M., Ryjacek, F., Hobza, P. (2006) *Chem. Eur. J.* **12**, 280 -290.

37. Caldwell, J. W., Kollman, P. A. (1995) *J. Phys. Chem.* **99**, 6208-6219.

38. Yeh, I.-C., Berkowitz, M. L. (1995) *J. Chem. Phys.* **111**, 3155-3162.

**Figure captions**

**Figure 1:** Born-Oppenheimer potential energies corresponding to NVT (at 270 K) on-the-fly trajectories of Zwitterionic systems containing an $H_3O^+$, $OH^-$ ion pair (black), and of corresponding neutral liquid $H_2O$ systems without ions (red). (A) A ~11 A thick slab of water in a two-dimensional periodic box. (B) A cubic box of water, with 3D periodic boundaries. Arrows mark the time of the ion-pair recombination; note subsequent lowering of the energy in the black curve of panel (B), and the absence thereof in panel (A). In panel (A), the mean energies of the system with the ion-pair, and of the neutral system, were -1236.794(0.017) and -1236.791(0.022) Hartree, respectively; (the numbers in the parentheses denote standard deviation). In panel (B), the corresponding energies were -1099.363( 0.0180) and -1099.413(0.0180), respectively. In the plots, the zero of the energy was shifted and the units were transformed to kcal/mol. The calculated mean energy differences between the Zwitterionic and neutral systems are -0.003 Hartree=-2±18 kcal/mol, and 0.05 Hartree=31±16 kcal/mol, for panels (A), and (B), respectively.

**Figure 2:** A typical snapshot from a molecular dynamics simulation depicting a surface bound $H_3O^+$ (red & white) and bulk $OH^-$ (orange & white) in an aqueous slab (blue & white). The two neighbouring periodic images of the solvent next to the unit cell are also depicted (shaded representation).

**Figure 3:** Spectroscopic signatures of proton activity using isotopic scrambling: on the left, isotopic exchange from surface proton hopping is reflected by loss ($D_2O$: 2725 $cm^{-1}$) and gain (HDO: 2712 $cm^{-1}$) of intensity of the bands of unique surface-dangling O-D bonds, while interior proton motion (right panel) causes a much slower conversion of the isolated-$D_2O$ doublet (2448 and 2370 $cm^{-1}$) to bands of an HDO pair having two coupled OD bonds in tandem. The prominent HDO singlet (2420 $cm^{-1}$) is produced by subsequent HDO rotation from passage of an orientational defect that decouples the O-D bonds *(17)*.

For the ice nanocrystal interior, the passage of orientational defects is fast compared to proton hopping *(17)* so the bands of the coupled HDO (2442 and 2400 $cm^{-1}$) are hidden throughout by the more intense isolated-HDO band at 2420 $cm^{-1}$. Less than a minute is required to complete the surface exchange at 140 K, while 30 minutes at 145 K is required to convert most of the interior $D_2O$ to HDO.

**Figure 4:** Graphical representation of interior and surface H-D exchange with time for an $H_2O$ ice aerosol, with ~10% D content, in He(g) at 128K. The plots show the percent loss of the interior $D_2O$ asymmetric- stretch band intensity (#) and the simultaneous diminution of the normalized peak intensity of the free-O-D surface band of $D_2O$ (*). Lines connecting data points are included as an aid to viewing.

**Figure 1:**

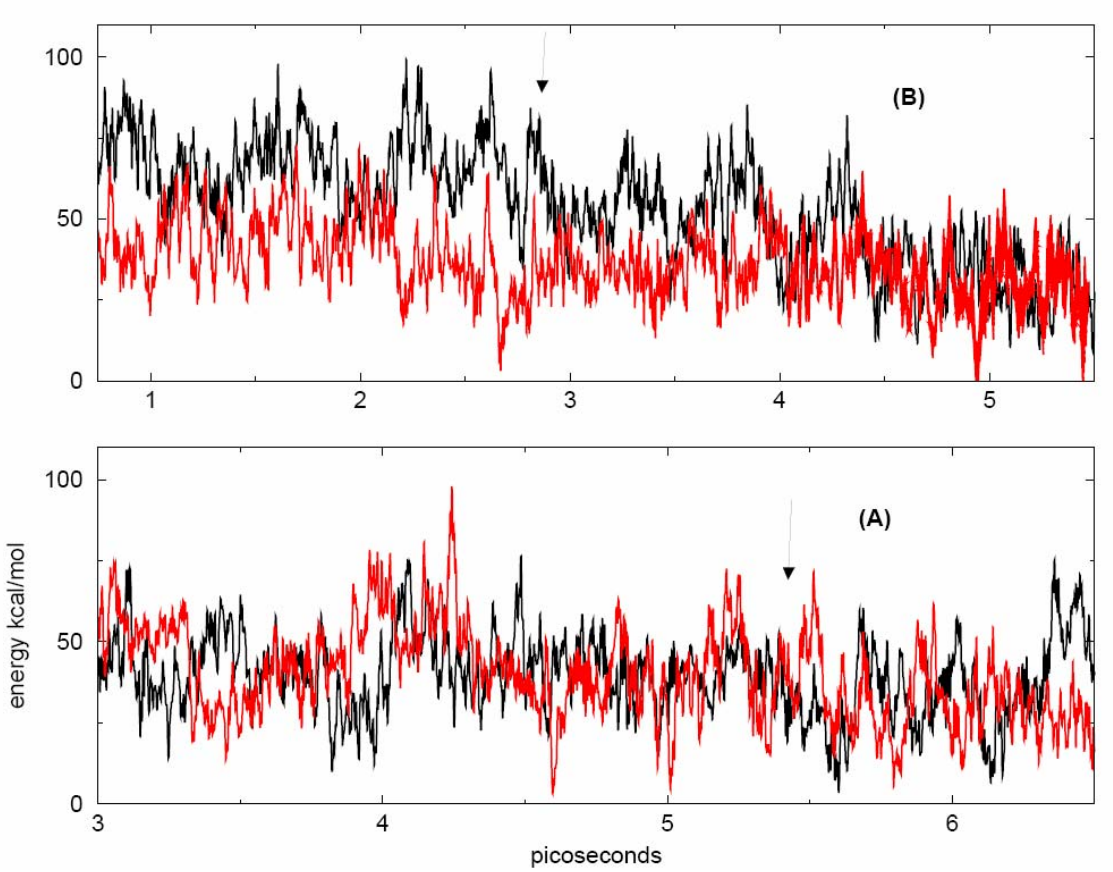

**Figure 2:**

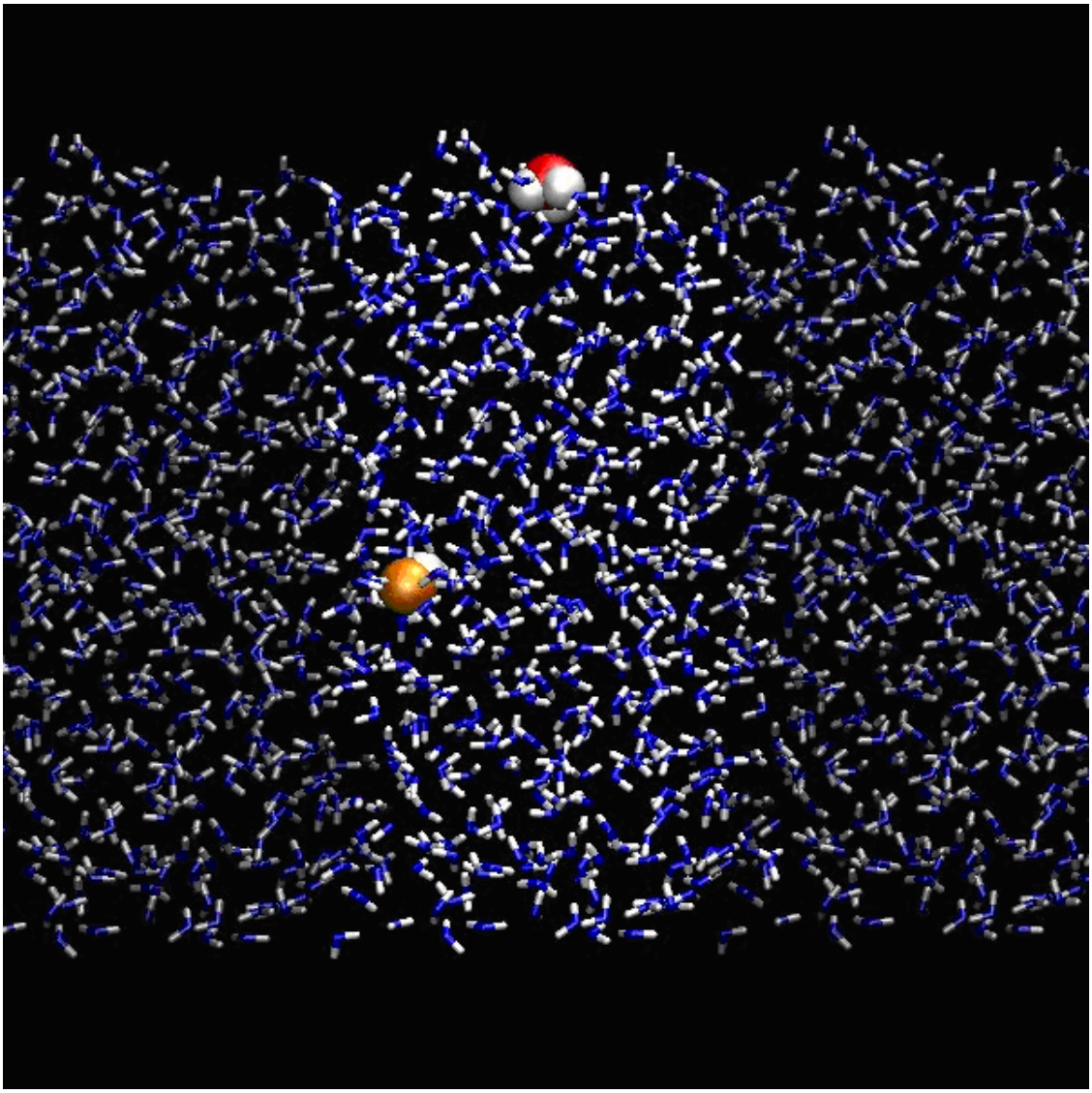

**Figure 3:**

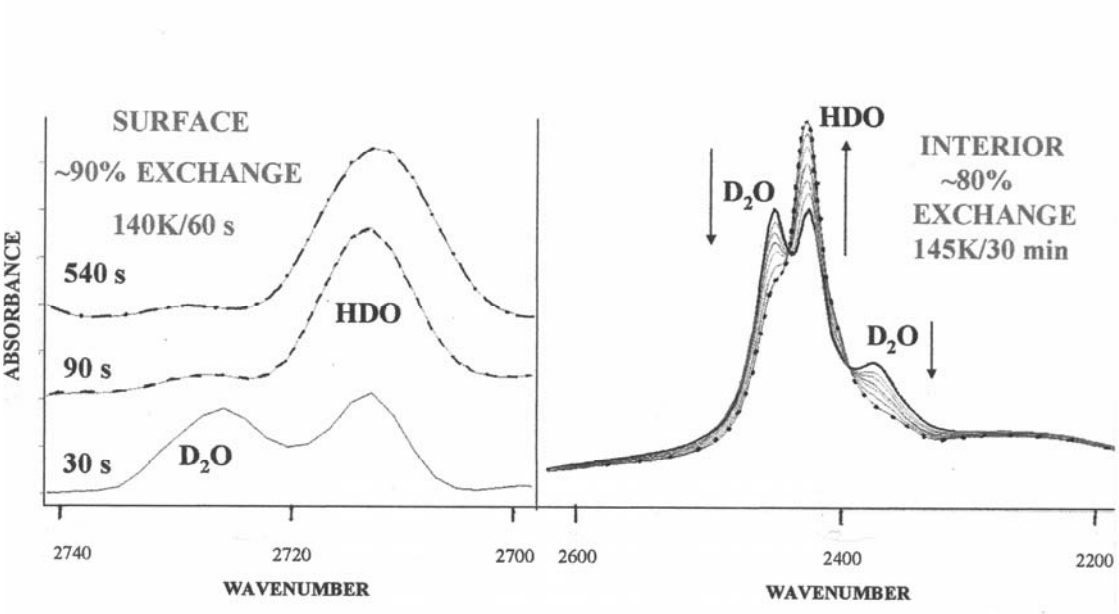
SURFACE
~90% EXCHANGE
140K/60 s
540 s
HDO
90 s
30 s
D2O
ABSORBANCE
2740
2720
2700
WAVENUMBER
HDO
D2O
INTERIOR
~80%
EXCHANGE
145K/30 min
D2O
2600
2400
2200
WAVENUMBER

**Figure 4:**

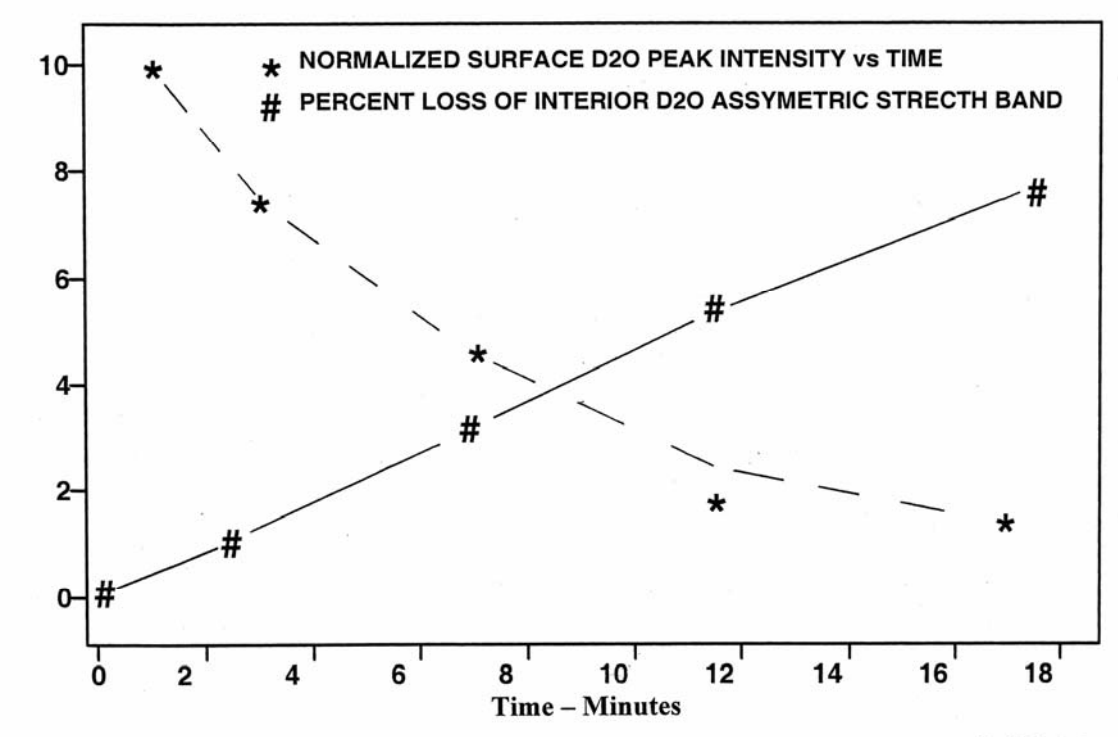
* NORMALIZED SURFACE D2O PEAK INTENSITY vs TIME
# PERCENT LOSS OF INTERIOR D2O ASSYMETRIC STRECTH BAND
10
8
6
4
2
0
0
2
4
6
8
10
12
14
16
18
Time – Minutes